CRREL REPORT 89-16

US Army Corps of Engineers
Cold Regions Research & Engineering Laboratory

4

Physical and optical properties of falling snow

For conversion of SI metric units to U.S./British customary units of measurement consult ASTM Standard E380, Metric Practice Guide, *published by the American Society for Testing and Materials, 1916 Race St., Philadelphia, Pa. 19103.*

Cover: Scattering of searchlight beam in falling snow.

CRREL Report 89-16

July 1989

Physical and optical properties of falling snow

Gary Koh

Prepared for
OFFICE OF THE CHIEF OF ENGINEERS

UNCLASSIFIED

SECURITY CLASSIFICATION OF THIS PAGE

REPORT DOCUMENTATION PAGE

Form Approved
OMB NO. 0704-0188
Exp. Date Jun 30, 1986

1a. REPORT SECURITY CLASSIFICATION
Unclassified

1B. RESTRICTIVE MARKINGS

2a. SECURITY CLASSIFICATION AUTHORITY

3. DISTRIBUTION/AVAILABILITY OF REPORT
Approved for public release; distribution is unlimited.

2b. DECLASSIFICATION/DOWNGRADING SCHEDULE

4. PERFORMING ORGANIZATION REPORT NUMBER(S)
CRREL Report 89-16

5 MONITORING ORGANIZATION REPORT NUMBER(S)

6a. NAME OF PERFORMING ORGANIZATION
U.S. Army Cold Regions Research and Engineering Laboratory

6b. OFFICE SYMBOL (if applicable)
CECRL

7a. NAME OF MONITORING ORGANIZATION
Office of the Chief of Engineers

6c. ADDRESS (City, State, and ZIP Code)
72 Lyme Road
Hanover, N.H. 03755-1290

7b ADDRESS (City, State, and ZIP Code)
Washington, D.C. 20314

8a. NAME OF FUNDING/SPONSORING ORGANIZATION

8b. OFFICE SYMBOL (if applicable)

9. PROCUREMENT INSTRUMENT IDENTIFICATION NUMBER

8c. ADDRESS (City, State, and ZIP Code)

10. SOURCE OF FUNDING NUMBERS

PROGRAM ELEMENT NO.	PROJECT NO	TASK NO.	WORK UNIT ACCESSION NO.
6.11.02A	4A161102 AT24	FS	003

11. TITLE (Include Security Classification)
Physical and Optical Properties of Falling Snow

12. PERSONAL AUTHOR(S)
Koh, Gary

13a. TYPE OF REPORT	13b. TIME COVERED FROM ____ TO ____	14. DATE OF REPORT (Year, Month, Day)	15. PAGE COUNT
		July 1989	28

16. SUPPLEMENTARY NOTATION

17. COSATI CODES		
FIELD	GROUP	SUB-GROUP

18. SUBJECT TERMS (Continue on reverse if necessary and identify by block number)
Electro-optical sensors; Falling snow; Detection (KT)
Extinction coefficient; Winter warfare;

19. ABSTRACT (Continue on reverse if necessary and identify by block number)
The physical and the optical properties of falling snow have been investigated during a series of winter tests (SNOW experiments). The techniques for measuring the physical properties of falling snow are described and a review of the empirical and the theoretical models for describing the extinction of visible and infrared radiation by falling snow is presented. The utility of these findings for the evaluation of electro-optical sensor performance in a winter environment is examined. Keywords:

20. DISTRIBUTION/AVAILABILITY OF ABSTRACT
☒ UNCLASSIFIED/UNLIMITED ☐ SAME AS RPT ☐ DTIC USERS

21 ABSTRACT SECURITY CLASSIFICATION
Unclassified

22a. NAME OF RESPONSIBLE INDIVIDUAL	22b. TELEPHONE (Include Area Code)	22c. OFFICE SYMBOL
Gary Koh	603-646-4100	CECRL-RG

DD FORM 1473, 84 MAR 83 APR edition may be used until exhausted.
All other editions are obsolete.

SECURITY CLASSIFICATION OF THIS PAGE

UNCLASSIFIED

PREFACE

This report was prepared by Gary Koh, Research Physical Scientist, Geophysical Sciences Branch, Research Division, U.S. Army Cold Regions Research and Engineering Laboratory. Funding for this research was provided by DA Project 4A161102AT24, *Research in Snow, Ice and Frozen Ground*; Task Area FS, *Fire Support*; Work Unit 003, *Microstructure of Hydrometeors.*

The author thanks Harold W. O'Brien and James Lacombe of CRREL for their suggestions and technical reviews of this report.

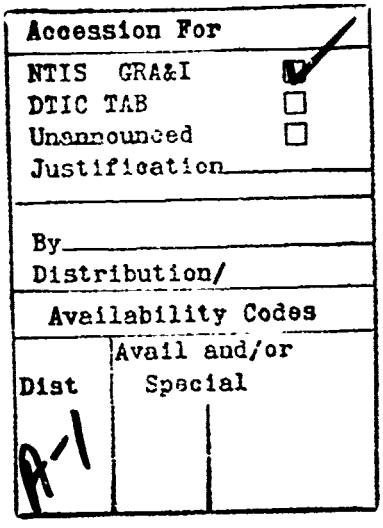

CONTENTS

ILLUSTRATIONS

Figure

TABLES

Physical and Optical Properties of Falling Snow

GARY KOH

INTRODUCTION

Many military electro-optical devices detect visible and infrared radiation that is emitted or reflected by distant targets. The performance of these electro-optical devices that rely on the propagation of optical energy between two points in space is largely dependent on the atmospheric conditions. Snow in the atmosphere scatters and absorbs visible and infrared radiation. This reduces the energy reaching the sensor of an electro-optical system or reduces the target/background contrast, or both. As a result, many electro-optical systems become ineffective even during periods of light snowfall. Investigations of the physical and optical properties of falling snow are necessary to evaluate the performance degradation of electro-optical devices in a winter environment.

The extinction coefficient is a measure of the attenuation of radiation as it propagates through the atmosphere. The effects of falling snow on the attenuation of optical radiation were investigated during a series of winter experiments (SNOW tests). Extensive transmission measurements at several infrared and visible wavelengths were made in conjunction with detailed measurements characterizing the properties of falling snow. These tests have led to the refinement of empirical and theoretical models for predicting the extinction of visible and infrared radiation by falling snow and also have led to improved techniques for characterizing the properties of snowfall. Although much progress was made during the SNOW tests, our knowledge of the physical and optical properties of falling snow remains incomplete. This report reviews what is known and is intended to provide guidelines for future research, and also to provide engineering and design guidelines for developing efficient methods to predict and improve the performance of electro-optical systems in a snow environment.

PROPERTIES OF FALLING SNOW

The major obstacle in the study of optical energy transmission through falling snow is the complex and diverse properties of snow particles. Snowstorms occur under diverse meteorological conditions so that snow particles of different size, shape and amount are generated. These snowfall properties must be known in order to develop models for predicting the transmission of visible and infrared radiation through falling snow. The properties of falling snow observed during the SNOW tests and the techniques used to measure these properties are presented.

Snow crystal type

During their initial growth phase, snow particles possess hexagonal plane and prismatic shapes. These hexagonal forms are maintained as long as the growth takes place by vapor diffusion. The shapes of these crystals that grow strictly by diffusion are dependent on the ambient temperature and humidity (Table 1). As these particles grow and become large enough to precipitate, nondiffusive growth mechanisms such as riming (accumulation of cloud droplets) and aggregation produce more complicated snow structures. Fragmented snow particles are frequently observed, which suggests that the snow particles are also modified by collision or other breakup mechanisms. The resulting variety of snow particle shapes is evident from the schematic representation of snow types introduced by Magono and Lee (1966), shown in Figure 1.

The detailed snow classification of Magono and Lee (1966) needs to be simplified for practical use. At present, a satisfactory snow classification scheme useful for transmission studies has not been developed. A reduced set of snow types should be devised based on similar physical or optical properties. A simple classification scheme

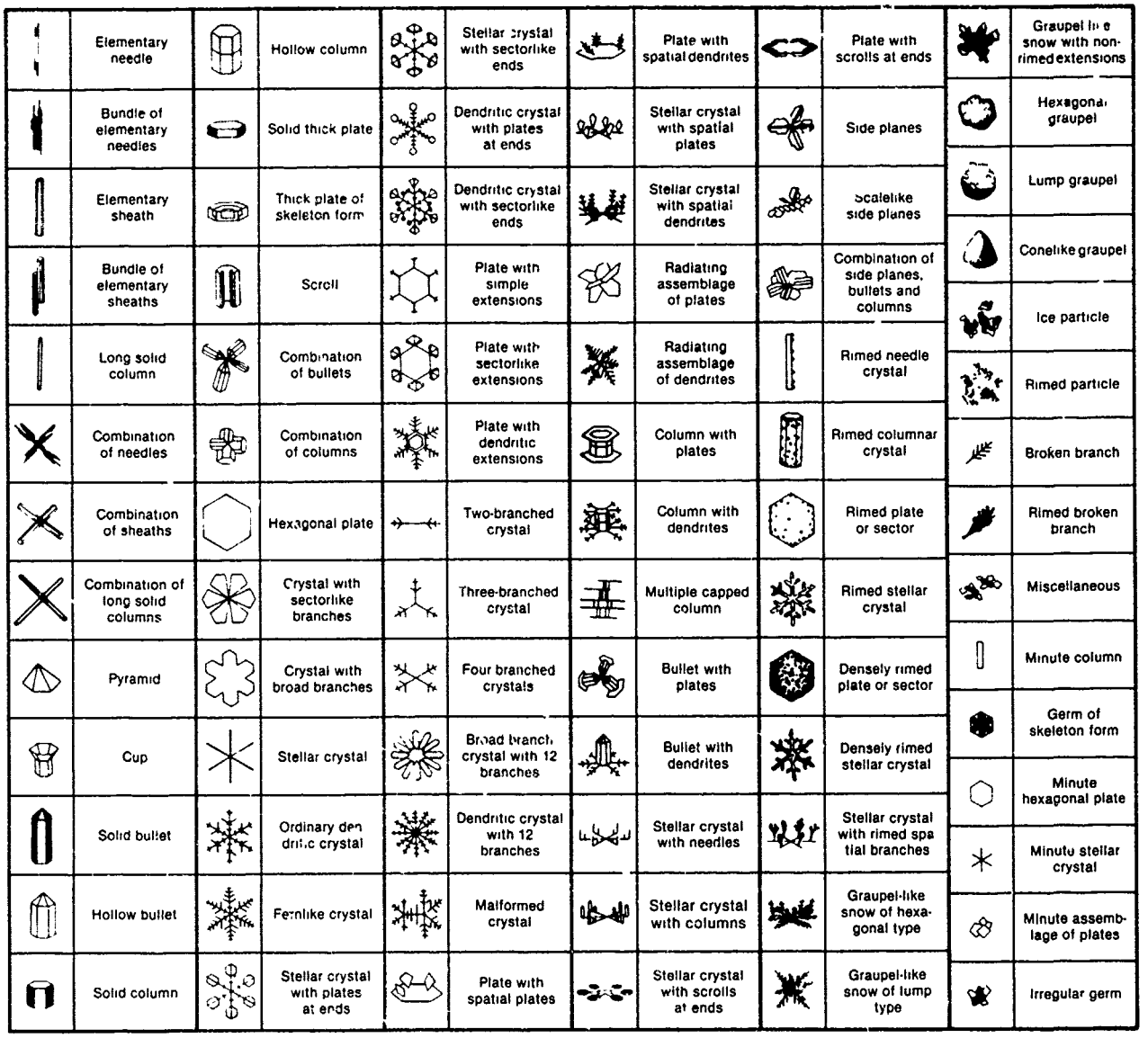

Figure 1. Schematic representation of various forms of snow and frozen particles (after Magono and Lee 1966).

Table 1. Snow crystal habit as a function of ambient conditions (°C) (Houghton 1986).

At or above water saturation		*Between ice and water saturation*	
0 to –4	plates	0 to –4	plates
–4 to –6	needles	–4 to –10	columns
–6 to –10	columns	–10 to –20	thick plates
–9 to –13	plates, sector plates		
–16 to –40	columns		
–13 to –17	stellars, dendrites		
–17 to –21	thick and sector plates		
–21 to –40	columns, plates, bullets		

describing the degrees of riming, aggregation and deviation from the spherical shape may be a useful starting point.

The Formvar replication technique (Schaefer 1941) is frequently used to analyze the shapes of snow particles. By use of this technique, plastic replicas of snow particles are made so that snow types can be determined at a later time in a laboratory. A replica is made by allowing a snow particle to fall on a surface that has been previously coated with a thin layer of replicating solution. The solution is made by dissolving plastic in a solvent (polyvinyl formal, better known as Formvar, dis-

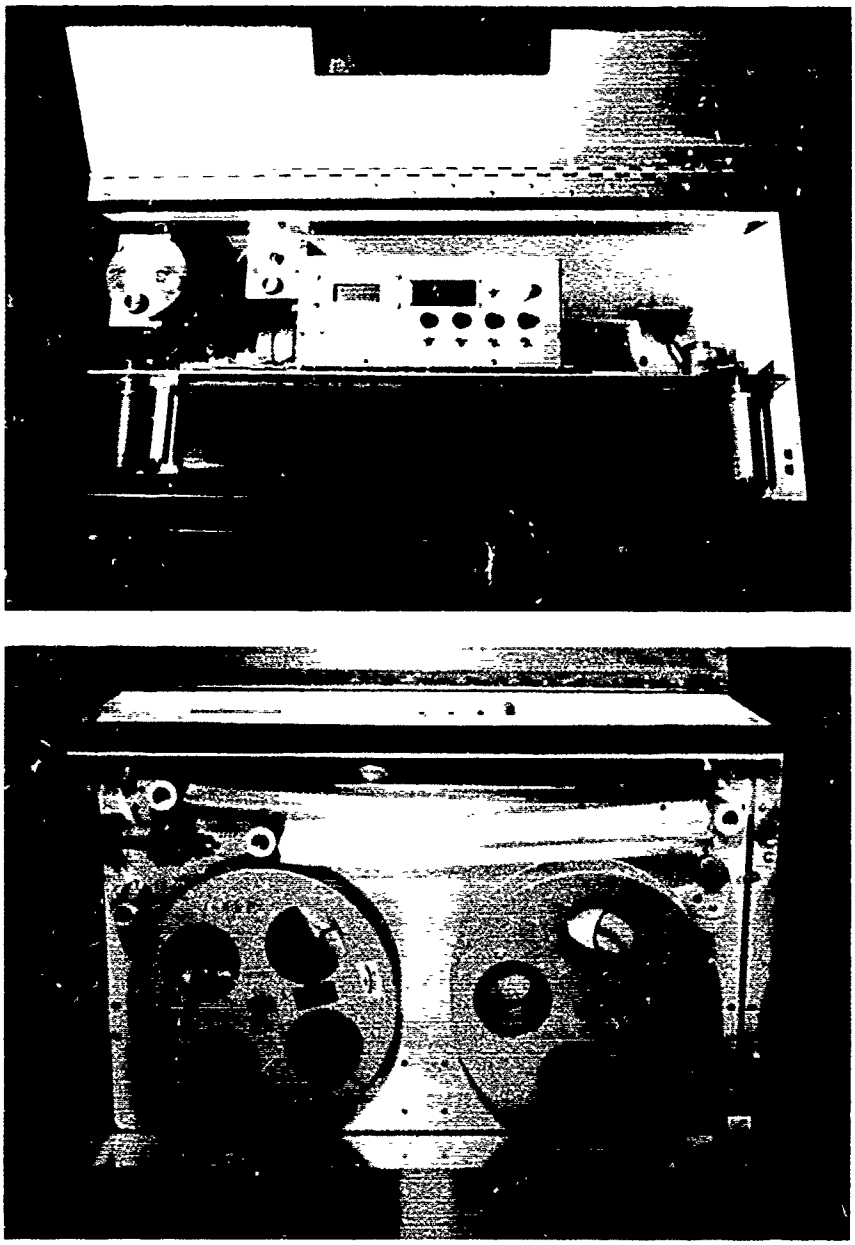

Figure 2. Top and front view of a continuous snow replicator showing the control panel and the film spools. Snow replicas are made on a clear 70-mm-wide motion film coated with Formvar solution.

solved in 1,2-dichloroethane, is commonly used). After a snow particle lands on the coated surface, the solution covers the snow through surface attraction. The solvent then evaporates, leaving the snow particle encased in a plastic film. After the snow sublimates, a hollow plastic replica of the original crystal remains.

Snow types can change, sometimes rapidly, during a snowfall. A continuous record of the snow type throughout a snowstorm can be maintained by automating the Formvar replication technique. Figure 2 shows a continuous replicator that was used during the SNOW tests. A clear 70-mm-wide motion film that has been coated with a thin layer of the Formvar solution moves and captures the snow particles as they fall through a sampling opening. The film is then wound onto a takeup reel after it has traveled a sufficient distance to ensure that the solvent has completely evaporated. A continuous length of film with the snow replicas is

produced that can be analyzed with any suitable magnifying instrument.

The analysis of snow types using the Formvar replication technique is tedious and time-consuming. Alternative methods for determining the snow types are desirable. Efforts are underway to relate the snowfall properties at ground level with specific synoptic meteorological conditions. For example, it may be possible to relate riming and aggregation to large-scale weather patterns. However, at present, the investigations of such relationships are limited and the numerical models describing precipitation formation are too simplistic to predict the detailed snowfall properties at specified locations.

Snow size distribution

The size distribution of snow particles is needed to calculate the attenuation of optical energy by falling snow. A widely used expression to model the snow size is the Gunn–Marshall distribution. Gunn and Marshall (1958) segregated their snowstorm data according to precipitation rate and used an exponential distribution to fit the results. The Gunn–Marshall distribution is expressed as

$$n(D_m) = n_m \exp(-\lambda_m \cdot D_m) \qquad (1)$$

where the distribution parameters

$$\lambda_m = 25.5 \cdot R_s^{-0.48} \cdot \text{mm}^{-1}$$

and

$$n_m = 3.8 \cdot 10^3 \cdot R_s^{-0.87} \text{ m}^{-3} \text{ mm}^{-1}$$

D_m is the diameter of a water drop to which a snow particle melts and R_s is the precipitation rate in millimeters of water per hour. Sekhon and Srivastava (1970) reanalyzed the data of Gunn and Marshall and of others and proposed that more consistent results could be achieved if the distributional parameters had the values

$$\lambda_m = 22.9 \cdot R_s^{-0.54} \text{ mm}^{-1}$$

and

$$n_m = 2.5 \cdot 10^3 \cdot R_s^{-0.94} \text{ m}^{-3} \text{ mm}^{-1}.$$

The simplicity of the exponential distribution makes it ideal for use in theoretical studies. The moments of the exponential distribution are given by

$$\int_0^\infty D_m^i n(D_m)\, dD_m = n_m \frac{\Gamma^{(i+1)}}{\lambda_m^{(i+1)}} \qquad (2)$$

where Γ is the gamma function. This equation implies that there is a correlation between the average snow size (first moment of the distribution) and the snow precipitation rate. However, the dependence of snow size distribution on precipitation rate alone may be an oversimplification when one considers the large variability in the structure of the snow particles. The observations of Feng and Grant (1982) on the correlation of the snow type, the number flux and the snow intensity indicate that the snow size is not necessarily dependent on the precipitation rate. The results obtained during the SNOW tests also indicate that the snow size is independent of the snow precipitation rate.

During the SNOW tests, 100 to 200 snow particles were replicated on 10 by 13 cm glass plates at the start of each hour during a snowstorm. The areas of the snow particles were measured by projecting the video images of the snow particles on a TV monitor and outlining them with a light pen. A computer was used to measure the outlined area of each particle and to compute its equivalent radius (the radius of a circle with the same area). Using this method the average snow sizes were obtained and compared with the snow mass concentration. Figure 3 shows that a correlation between snow size and snow mass concentration was not observed during the SNOW tests, which contradicts the exponential size distribution model

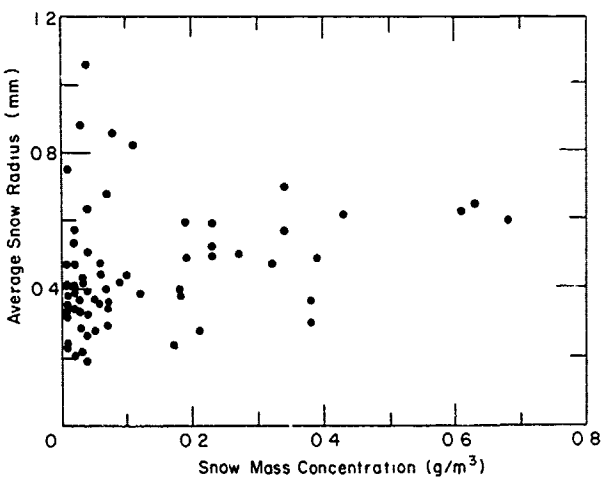

Figure 3. Relationship between the average snow size and the snow mass concentration. A correlation between snow size and snow intensity does not exist.

(although snow mass concentration is used instead of snow precipitation rate, the argument remains valid since a correlation exists between the two snowfall parameters). At the lower snowfall intensities, the average snow size ranged between 0.3 and 1.1 mm in radius. However, as the snowfall intensity increased, the average snow size was less than 0.8 mm.

The snow size distributions observed during the SNOW tests varied significantly and it was difficult to find suitable analytical expressions to model the snow size. The collected snow samples frequently contained several snow types with varying degrees of riming and aggregation, so the data could not be easily segregated according to snow type. Therefore, the snowstorms were segregated based on the average snow size, and the modified gamma distribution was used to describe the snow size distribution for each class of snowstorm. The modified gamma distribution is a three-parameter model expressed as

$$n(a) = \kappa \cdot a^{\alpha} \cdot \exp[(-\alpha/\gamma)(a/a_c)^{\gamma}] \qquad (3)$$

where $n(a)$ is a continuous and an integrable function of radius a. The shape of the distribution is governed by α (positive integer), γ (positive constant) and a_c (mode radius). The value κ is used to normalize the total number of particles in a unit volume and does not affect the shape of the distribution.

Figure 4 illustrates the modified gamma distribution fit for the composite size distributions for snowfalls whose average radii range from 0.2–0.7 mm. These size ranges accounted for approximately 90% of the snowfalls observed during the SNOW tests. These size distributions were obtained from snow particles that were replicated on a horizontal surface. To infer the size distribution in space (unit volume), the observed distributions must be divided by the fall velocity of the snow particles in each size interval. Since the snow fall velocity is not uniquely dependent on the size, errors are introduced when inferring the size distribution in space from the replication technique.

The segregation of the snow data based on the average size only provides a rough estimate of the actual distribution. The composite distributions do not adequately represent the snow size distribution for snowfall that is composed of large aggregates. A bimodal distribution is often observed as the number of the large aggregates increases. To more accurately represent the snow size distributions, an analytical expression that takes into account the bimodal distribution is required. At present, information on the size distribution of snow particles is limited and more studies are required to develop realistic models of the snow size.

To obtain more information about the snow size distribution, improved techniques for measuring snow particle sizes are needed. The available information on the snow sizes has, for the most part, been obtained using laborious methods such as replication or photography. To improve the snow measurement capability, Berger (1983) investi-

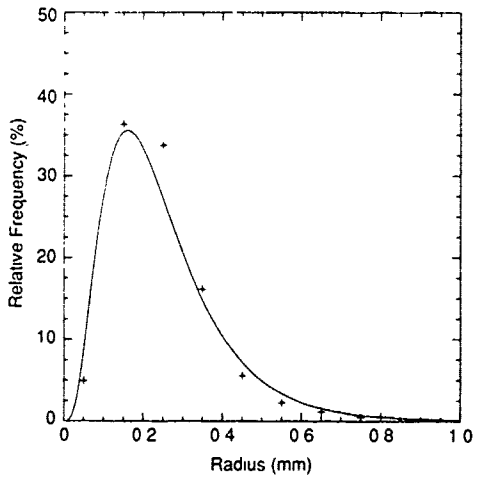

a. Average size 0.2–0.3 mm ($\alpha = 5$, $\gamma = 0.5$, $a_c = 0.15$).

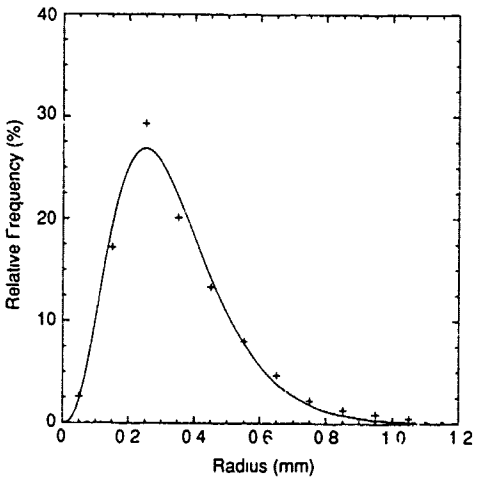

b. Average size 0.3–0.4 mm ($\alpha = 4$, $\gamma = 0.8$, $a_c = 0.25$).

Figure 4. Modified gamma distribution fit for composite snow size distributions. The data were segregated according to the average snow size.

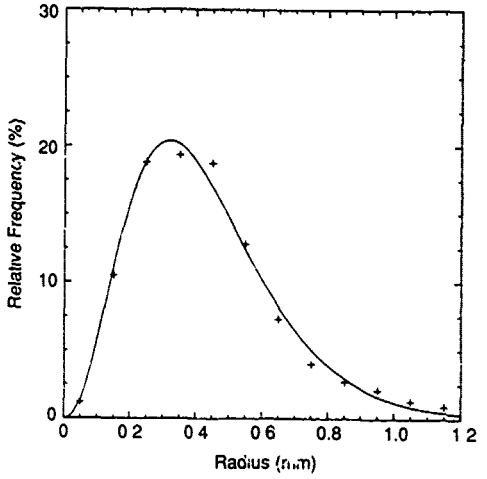

c. Average size 0.4–0.5 mm ($\alpha = 3$, $\gamma = 1.1$, $a_c = 0.32$).

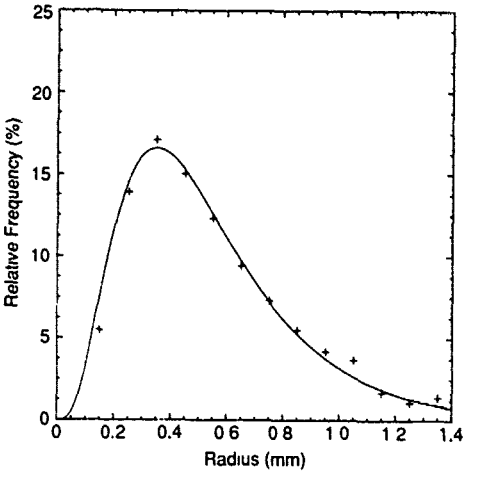

d. Average size 0.5–0.6 mm ($\alpha = 2$, $\gamma = 1.0$, $a_c = 0.35$).

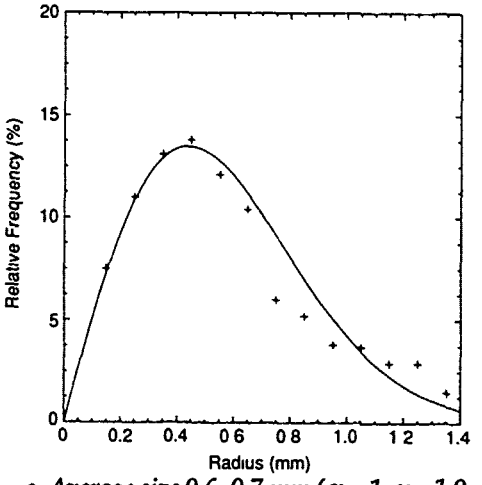

e. Average size 0.6–0.7 mm ($\alpha = 1$, $\gamma = 1.9$, $a_c = 0.45$).

Figure 4 (cont'd). Modified gamma distribution fit for composite snow size distributions. The data were segregated according to the average snow size.

gated the feasibility of using a PMS (Particle Measuring System) two-dimensional optical array imaging probe to measure the snow sizes during the SNOW tests. The imaging probe uses a linear array of photodiodes as a size-measuring grid in a shadowgraph-type manner. A particle entering the sample volume passes through a beam of light that produces a shadow on the photodiodes. The photodiodes are scanned at a known frequency to produce a digitized image of each particle. The data are in a form that can be easily managed with computer processing so that large amounts of data can be obtained with a minimum amount of attention. A schematic of the probe and some examples of digitized images of snow particles are shown in Figure 5.

The PMS probes were designed to be aircraft-mounted to measure the size of cloud and precipitating particles. For ground operations, the snow particles were aspirated into the sample volume at a known velocity (since the photodiodes are scanned at fixed frequency, the velocity of the particle as it passes the beam must be known). To interpret the data obtained from ground operations, the effect of the aspiration on the measurements of number concentration and size distribution of snow particles was investigated. The numerical studies by Norment (1986) and the experimental studies by Humphries (1985) and Holroyd (1986) on the effects of aspiration are not conclusive and more studies are required. When the PMS probes can be properly calibrated for the effect of aspiration, their ability to measure the snow sizes rapidly and continuously makes them ideal instruments for future snow size distribution studies.

Snow size versus ambient conditions

The average snow size (equivalent radius) observed during the SNOW tests generally ranged from 0.2 to 0.7 mm. The frequency distribution of the average size is shown in Figure 6. It was previously shown that the average snow size was not related to the snowfall intensity (Fig. 3). The relationships between the average snow size and the surface meteorological conditions measured during the SNOW tests were also investigated. Figures 7 and 8 illustrate the relationships of the average snow size to surface temperature (measured at 2-m height) and to relative humidity respectively. For snowfalls that occurred when the

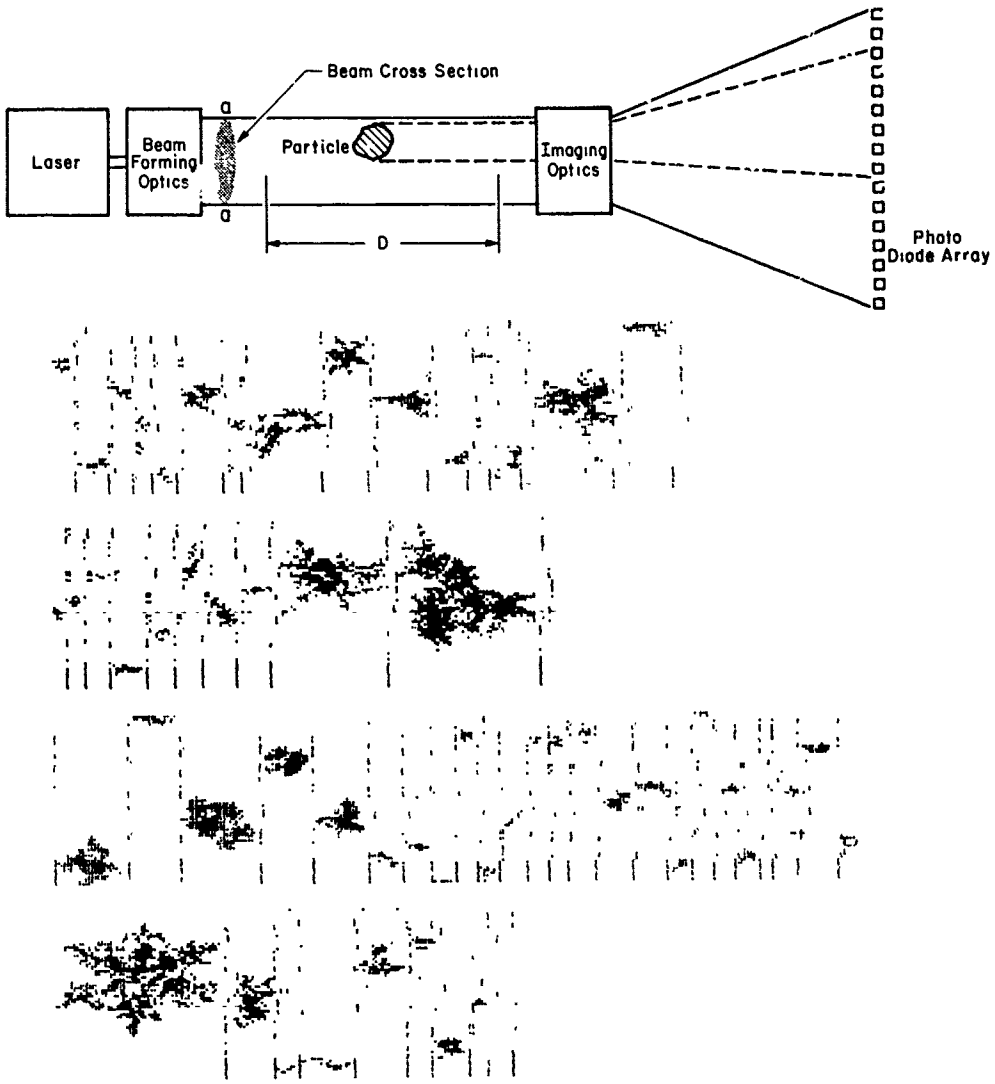

Figure 5. Schematic of a Particle Measuring System optical imaging probe and digitized images of snow particles (from Berger 1983).

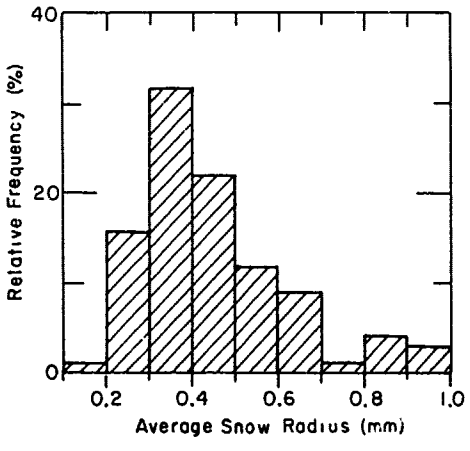

Figure 6. Distribution of the average snow size (equivalent radius) obtained from Formvar replicas.

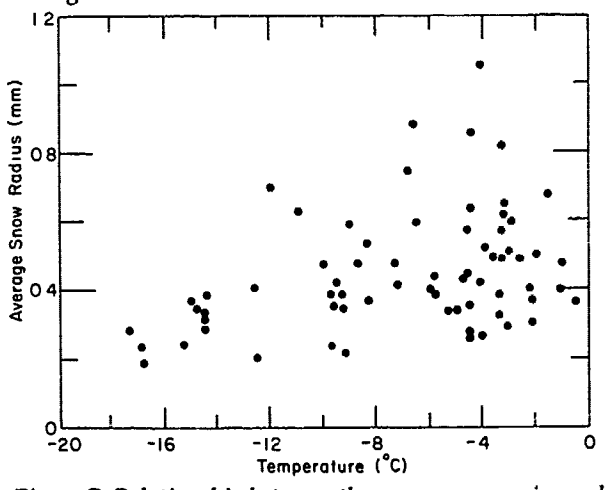

Figure 7. Relationship between the average snow size and the surface temperature.

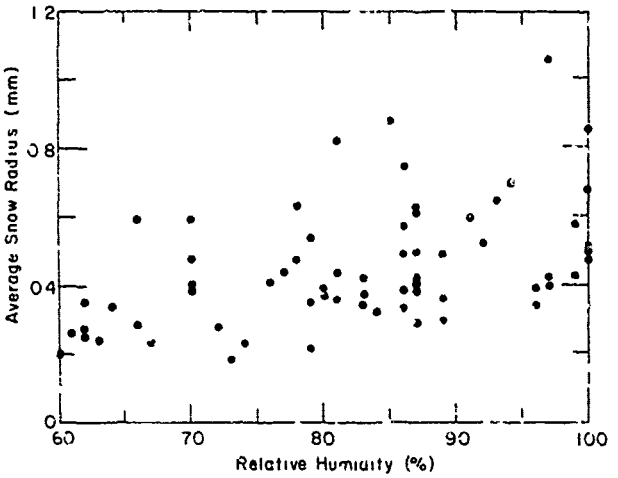

Figure 8. Relationship between the average snow size and the relative humidity.

surface temperature, T, was between –18 and 0°C, a linear regression of the data resulted in the following

$$\bar{a}\ (\text{mm}) = 0.6 + 0.02T\ . \qquad (4)$$

The relationship between snow size and relative humidity (RH is expressed using decimals) resulted in the following linear regression

$$\bar{a}\ (\text{mm}) = -0.33 + RH\ . \qquad (5)$$

Although the figures indicate that the snow sizes increase as the temperature and the humidity increase, the scatter in the data is such that the regression results may not be very meaningful.

Snow particle fall velocity

The fall velocities of snow particles are important when investigating the relationship between snow precipitation rate and snow extinction coefficient. Due to the diverse sizes and shapes of snow particles, a range of snow fall velocity exists. Numerous empirical relationships between the snow fall velocity and the snow type and size have been reported. Typically, the observed data are fitted by a power function of the type

$$v_s = a \cdot d_m^b \qquad (6)$$

where v_s is the fall velocity, d_m is the size of the snow particle and a and b are contants for a given type of snowfall (Jiusto and Bosworth 1971, Locatelli and Hobbs 1974).

Other empirical fits to the snow fall velocity data have also been reported. O'Brien (1970) analyzed the data of Nakaya (1954) and Magono (1951, 1953, 1954) and arrived at the following relationship

$$v_s = a \cdot d_m^n \cdot [\log_{10}(v_s \cdot d_m) + b] \qquad (7)$$

where a, b, and n are empirical constants that were chosen to fit the data. Suzuki et al. (1981) studied the relationship between the snow fall velocity and snow density, ρ_s(g/cm³), and observed the following:

$$v_s = 2.36 \cdot \rho_s^{0.3} \cdot d_m^{0.23}\ . \qquad (8)$$

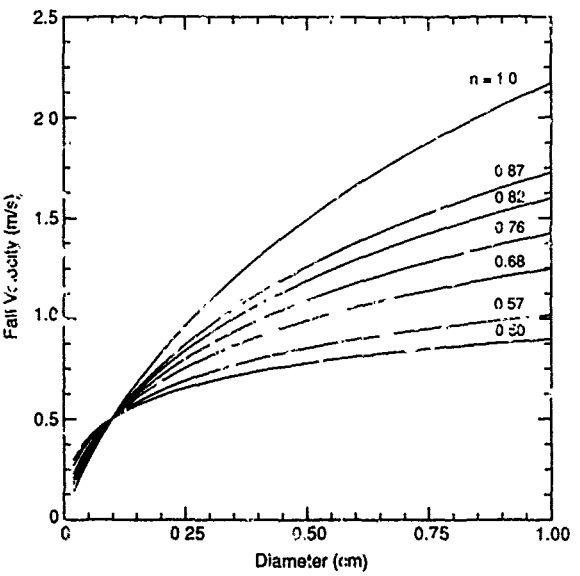

a. $v_s = -17.6 \cdot d_m^n\ [log_{10}(v_s \cdot d_m) - 4.57]$ *(after O'Brien 1970).*

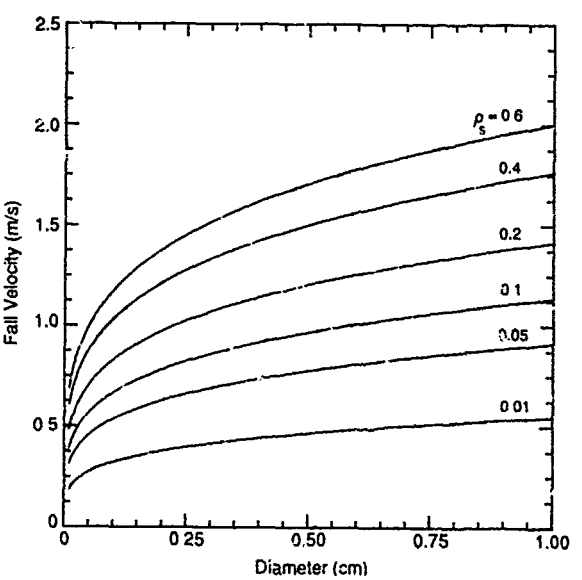

b. $v_s = 2.36 \cdot \rho_s^{0.3} \cdot d_m^{0.23}$ *(after Suzuki et al. 1981).*

Figure 9. Empirical relationships between snow fall velocity and size for different snow types.

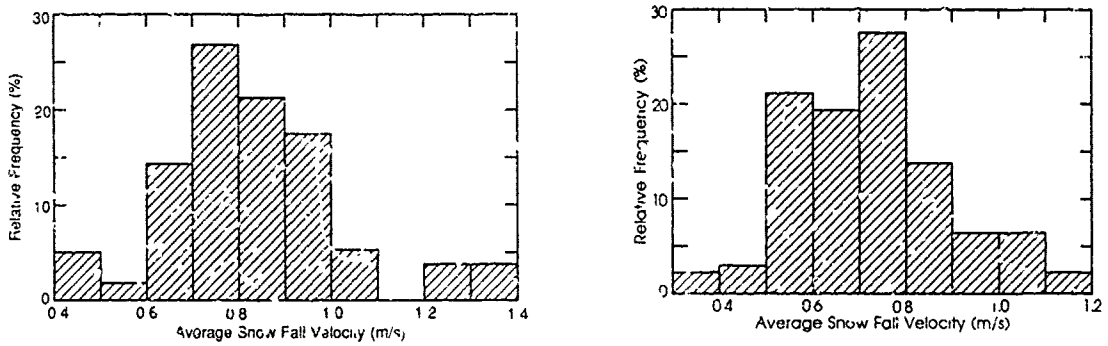

a. Mellor (1966). *b. Rosinski et al. (1983).*

Figure 10. Distribution of the average snow fall velocities.

Since the methods used to describe the size and to classify the snow type often vary among researchers, it is difficult to compare the results obtained by the different investigators. Figure 9 illustrates the empirical fits for different types of snowfall reported by O'Brien (1970) and Suzuki et al. (1981).

Mellor (1966) and Rosinski et al. (1983) observed the fall velocities of snow particles over a period of few minutes to find the average snow fall velocity. The average fall velocity reported by these investigators generally ranged from 0.4 to 1.1 m/s. The frequency distributions of the average fall velocities are shown in Figure 10. The results are very similar, and both distributions have the mode value of 0.75 m/s for the fall velocity.

During the SNOW tests, Berthel et al. (1983) measured snow particle fall velocities. Multiple images of a snow particle were recorded on a single video frame by illuminating the vertical fall with a strobe light. The fall velocity of individual particles was determined from the distance between the images and the known frequency of the strobe illumination. A power fit was used to relate the snow size and the fall velocity. They found that the snow fall velocities generally ranged between 0.5 and 2.0 m/s, which agreed well with the previously described empirical relationships.

Snow particle mass

The mass (or density) of individual snow particles is difficult to measure and large discrepancies exist among various investigators. The relationships of snow precipitation and snow mass concentration to the optical attenuation is greatly affected by the mass of the snow particles. Figure 11 shows the range of snow masses observed by

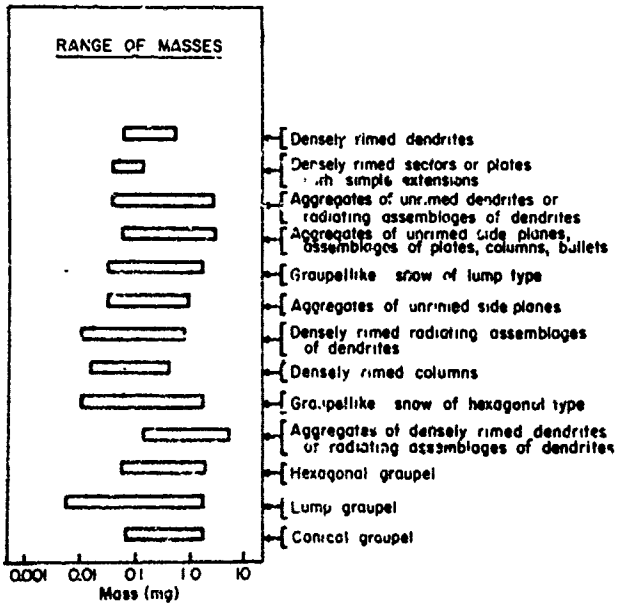

Figure 11. Range of snow masses for commonly observed snow types (after Locatelli and Hobbs 1974).

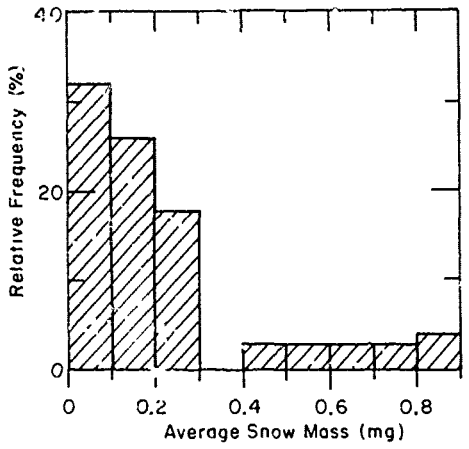

Figure 12. Distribution of the average snow mass (after Rosinski et al. 1983).

Locatelli and Hobbs (1974). The snow mass was determined by melting the snow particles in oil and measuring the melted droplet diameter. Rosinski et al. (1983) measured the average mass of snow particles during snowfall by both conductive titration and by weighing the individual particles. A histogram of the average mass observed by these investigators is shown in Figure 12. No attempt was made to measure the mass of individual snow particles during the SNOW tests.

Snow precipitation rate

The most common quantitative measure of the falling snow is the precipitation rate. This is typically measured by monitoring the amount of snow that falls through a horizontal surface sample area into a tipping-bucket or weighing-type device. These mechanical gauges have poor precision and time resolution, so they are inadequate to support electro-optical system performance tests where the short-term variations in the snowfall rate are important. Berthel et al. (1983) and Lacombe (1983) used electronic balances to improve the weighing technique for measuring the snow precipitation rate. They were able to reduce the average sampling time for measuring precipitation rate to 1 minute.

An optical technique for measuring snowfall rate, which may be more suitable than the electronic balance gauge for field applications, was investigated by Koh and Lacombe (1986). The optical gauge shown in Figure 13, which was originally designed to measure rain rates (Wang et al. 1980), was modified for operation in snow. The light source for the optical gauge is an infrared-emitting diode that is partially collimated. Snow particles falling through the sample area break the light beam to produce light intensity fluctuations on the receiver. The receiver output is passed through a bandpass filter (75–900 Hz), and its rms value is measured. This yields a slowly varying (10-s time constant) dc voltage proportional to the snow rate. Comparisons of the precipitation rates measured with an electronic balance gauge and an optical gauge have shown that the snow precipitation rate can be estimated within a factor of two using the optical gauge. The loss of accuracy in snow rate measurement using the optical technique is compensated for by its simplicity (virtually no maintenance is required) and improved

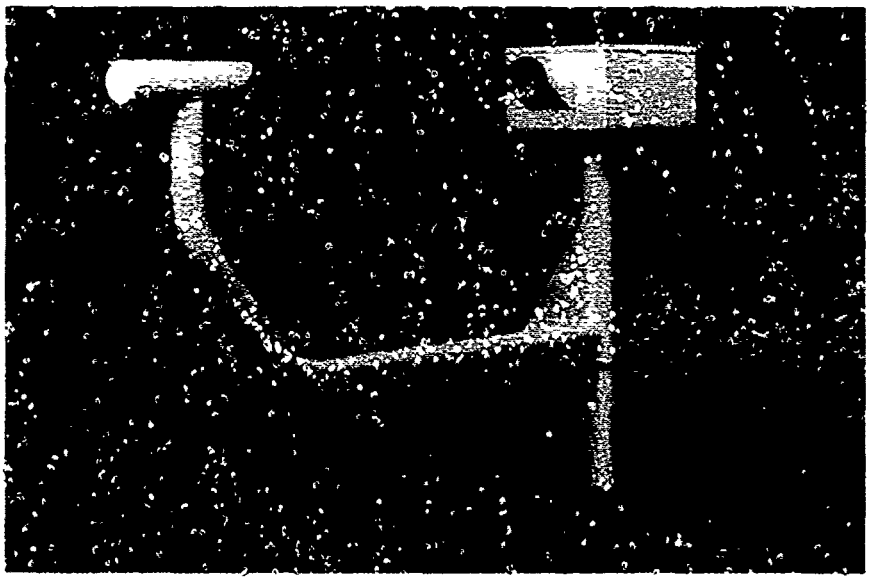

Figure 13. Optical gauge for measuring snow precipitation rate.

time resolution over conventional snow gauges. The accuracy of snow rate measurement can be improved by segregating the data according to snow types. Studies are being conducted to determine the feasibility of identifying the snow types using the optical gauge.

Snow mass concentration

The snow mass concentration is the mass of snow per unit volume of the atmosphere during a snowstorm. Stallabrass (1976) introduced a direct means of measuring the snow mass concentration that was later improved by Lacombe (1983). Figure 14 shows the device used to measure the snow mass concentration during the SNOW tests. A collection head mounted on an arm rotating in a horizontal plane sweeps a known volume of air and the air–snow mixture enters a collection orifice. The snow particles are then separated from the air, melted and forced through a needle by centrifugal force. Equally sized droplets form at the needle tip and are photoelectrically counted as they separate from the needle and pass between an infrared-emitting diode and a phototransistor. The mass of the droplet is calculated from a force-balance analysis that relates centrifugal and surface tension forces. Summing the number of droplets over a given time period provides a measure of the snow mass concentration.

Accurate measurement of snow mass concentration requires a high collection efficiency rate for the collection inlet. A numerical study by Norment (1986) determined the sampling efficiency of the mass concentration measuring instruments to be excellent over a comprehensive size range of water drops (20- to 1000-μm diameter) and hexagonal ice plates (40- to 700-μm plate diameter). The operation of these instruments during the SNOW tests demonstrated that the snow mass concentration can be measured over extended time periods and that the changes in snow intensity can be rapidly monitored (once every minute), making this instrument a valuable tool for characterizing the snow environment during tests of electro-optical system performance.

Relationship between mass concentration and precipitation rate

The relationship between the snow mass concentration M_s and the snow precipitation rate R_s can be approximated by

$$M_S = R_S / \bar{v}_S \qquad (9)$$

where $\bar{v}_s$ is some representative snow fall velocity. Since R_s is commonly measured, the ability to estimate M_s from R_s measurement is of practical interest. Mellor (1966, 1983) measured R_s and the average snow fall velocity to estimate M_s. The relationship between M_s(g/m^3) and R_s (mm/hr) was described by the following relationship

$$M_S = 0.32 \cdot R_S^{0.9} \qquad (10)$$

Koh et al. (1988) directly measured M_s and R_s and the linear regression fit to the data resulted in the following M_s to R_s relationships

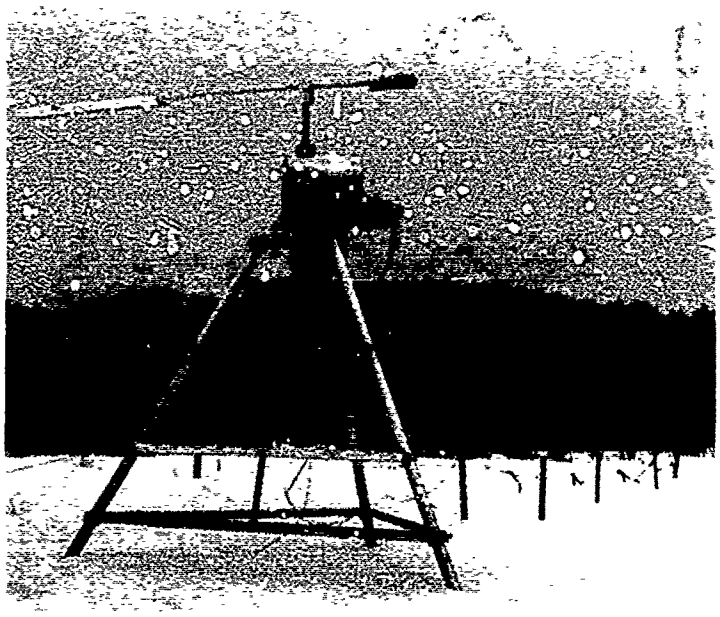

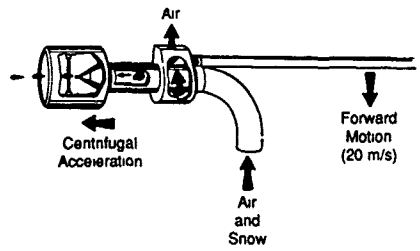

Figure 14. Instrument for measuring the snow mass concentration and schematic of its collection head (from Lacombe 1981)

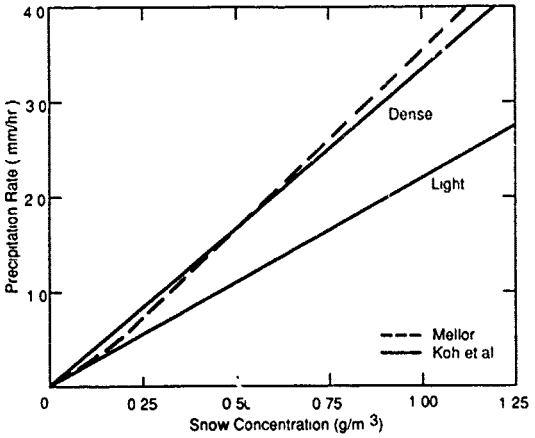

Figure 15. Relationship between the snow precipitation rate and the snow mass concentration.

$$M_s = 0.30 \cdot R_s \text{ ("dense" snow)} \qquad (11a)$$

$$M_s = 0.47 \cdot R_s \text{ ("light" snow)} . \qquad (11b)$$

The "dense" and "light" classifications refer to the bulk density of snow crystals. Snowstorms composed of ice pellets, needles, columns and rimed particles were classified as "dense" snow. Snow particles with cavities and irregularities in the external crystal structure, such as aggregates of snow particles and spatial dendrites, were classified as "light" snow. Although the classification is subjective, the M_s to R_s relationships for the two types differ. Figure 15 illustrates the M_s to R_s relationships observed by Mellor (1983) and Koh et al. (1988).

THEORY OF EXTINCTION

The amount of transmitted optical energy received by a detector located downstream is reduced during a snowstorm. This process, called extinction, is caused by the energy redistribution of the transmitted radiation due to scattering and absorption by the snow particles along the transmission path. The extinction characteristic of snow particles is described in terms of the extinction coefficient B_{ext}, which is expressed as

$$B_{ext} = \int_0^\infty [C_{sca}(a) + C_{abs}(a)]\, n(a)\, da . \qquad (12a)$$

C_{sca} and C_{abs} represent the scattering and the absorption cross sections, respectively, and $n(a)$ is the number of particles per unit volume with sizes between a and $a+da$. The total energy scattered in all directions and the total energy absorbed inside a particle are equal to the energy of the incident wave falling on the areas C_{sca} and C_{abs} respectively. The extinction cross section C_{ext} is defined as $C_{sca}+C_{abs}$.

The dimensions of the snow particles are much larger than the visible and infrared wavelengths; therefore, short-wavelength limit approximation can be used to determine the extinction cross section. In this approximation, the extinction cross section is equal to twice the geometrical cross section (van de Hulst 1957). Equation 12a can therefore be simplified to

$$B_{ext} = 2\int_0^\infty \pi\, a^2\, n(a)\, da \qquad (12b)$$

where πa^2 is the area of a snow particle projected normal to the incident beam. This seeming contradiction, that a large particle removes from the incident radiation twice the amount of energy it can intercept, is referred to as the extinction paradox.

The extinction paradox can be explained using geometrical optics and physical optics approximations. The geometrical optics approximation (subdividing the incident radiation into a large number of rays and using the Fresnel equation and Snell's law to determine the interaction at the boundaries) indicates that the energy incident on the geometrical cross section πa^2 is either reflected or refracted. The refracted energy is either absorbed or it is refracted out of the particle. In addition to this reflected and refracted cross section πa^2, the diffraction also contributes to the total extinction.

The effects of diffraction can not be explained using geometrical optics; therefore, a physical optics solution (scalar diffraction theory) is required. Invoking the "Babinet Principle," which states that the diffraction patterns are similar when observed behind either an aperture or an obstacle of the same shape and size, one can show that the amount of diffracted energy is also equal to the amount of energy incident on the geometrical cross section πa^2. The combined effects of reflection, refraction and diffraction result in the extinction cross section of $2\pi a^2$.

Once the extinction coefficient is known, the variation of the radiation intensity I along the propagation path L can be determined using the relationship

$$dI = -I \cdot B_{ext} \cdot dL . \qquad (13)$$

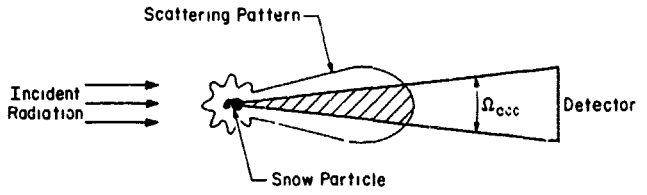

Figure 16. Illustration of the forward-scattered light measured by a detector. Measured extinction is less than the theoretical by the amount of the forward-scattered light contained in the shaded region.

Integration of this equation yields the familiar Beer-Lambert relationship for the "theoretical" transmittance T (the reason for specifying "theoretical" is explained later) through the atmosphere

$$T = \frac{I}{I_0} = \exp(-B_{ext} \cdot L) \qquad (14)$$

where I_0 is the intensity at the start of the path and I is the intensity at distance L.

Equation 14 is valid if the contribution to the received power from forward scattering is negligible. In actual practice, since all detectors have a nonzero field of view, a portion of the radiation scattered in the forward direction contributes to the received power. The effect of forward scattering is illustrated in Figure 16. The shaded area represents the forward-scattered radiation entering the acceptance angle Ω_{acc} of a detector. The "theoretical" prediction for transmittance is always less than the "measured" transmittance, since eq 14 does not account for forward scattering contribution to the measured transmittance. The difference between the "measured" and the "theoretical" values is determined by the detector size and the amount of forward-scattered radiation.

This brief overview has been presented to show that the extinction coefficient, the angular distribution of scattered radiation, and the geometries of the transmitted beam and the receiver are required to predict the amount of radiation measured by any electro-optical device.

Comparison of visible and infrared transmission

The transmission data obtained during the SNOW tests indicate that snow is slightly more transparent to visible light than to infrared radiation. Typical visible and infrared transmission data through the falling snow are shown in Figure 17. Transmission in the far-infrared (8- to 14-μm) and mid-infrared (3- to 5-μm) regions is lower than in the visible regions. The transmission at the near-infrared (1.06 μm) region is slightly higher than at the visible wavelength (in most cases, visible transmission through snowfall is better than 1.06 μm regions). These measured transmission results are contrary to eq 12b, which indicates that extinction by snow particles is independent of wavelength in the visible and infrared regions. Table 2 shows some of the previously reported relationships between infrared and visible transmission.

The observed wavelength dependence appears to be the result of the increase in the scattering in the near forward direction at the shorter wavelengths. As the ratio of the particle size to the wavelength increases, more of the scattered radiation is concentrated in the forward direction. Therefore, the contribution of the narrow-angle forward scattering into the receiver is greater at the shorter wavelengths. The effect of forward scattering on the measured transmission is discussed in the next section.

Forward-scattering correction

The angular distribution of the light scattered by irregularly shaped particles is not known. Therefore, calculations of the forward-scattering correction to extinction in falling snow have for the most part been based on the theories of scattering by spherical particles. Miller (1978), Mill and Shettle (1983) and Seagraves (1983) used spherical approximation for snow particles and used the Fraunhofer diffraction theory to calculate the intensity

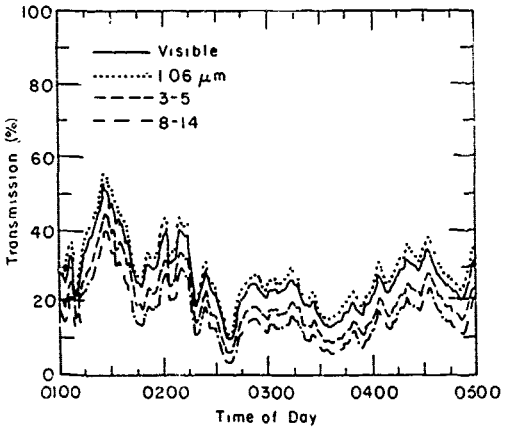

Figure 17. Comparison of the visible and infrared transmission data through falling snow. Snow is slightly more transparent to visible light than to infrared radiation.

Table 2. Relationships between visible and infrared extinction in falling snow (after Seagraves 1986).

$B_{ext(10.6\ \mu m)} = 1.4 \cdot B_{ext(0.63\ \mu m)}$	Bisyarin et al. (1971)
$B_{ext(10.6)} = 1.38 \cdot B_{ext(0.63)}$	Bisyarin et al. (1973
$B_{ext(3.0\text{-}5.0)} = 1.05 \cdot B_{ext(0.55)}^{1.05}$	Duncan (1981); Sola and Bergmann (1977)
$B_{ext(8.0\text{-}12.0)} = 1.30\ B_{ext(0.55)}^{0.99}$	
$B_{ext(8.0\text{-}12.0)} = 1.25\ B_{ext(visible)}^{0.90}$	
$B_{ext(10.4)} = 1.42 \cdot B_{ext(0.55)}$	Lacombe and O Brien (1982)
$B_{ext(3.0)} = 1.43 \cdot B_{ext(0.55)}$	
$B_{ext(1.06)} = 1.06 \cdot B_{ext(0.55)}$	
$B_{ext(10.5)} = 1.18 \cdot B_{ext(0.55)}$	Seagraves and Ebersole (1983)

of light scattered in the near-forward direction. Using the Fraunhoher diffraction theory, the intensity in the forward direction can be expressed as

$$\frac{dC_{sca}}{d\Omega} = \frac{x^4}{k^2}\left[\frac{J_1(x\sin\theta)}{x\sin\theta}\right]^2 \qquad (15)$$

where the differential cross section $dC_{sca}/d\Omega$ is the amount of radiation scattered per unit incident radiation into a unit solid angle about a given direction, k is the wave number ($2\pi/\lambda$), x is the size parameter (ka), and J_1 is the first-order Bessel function. θ is the scattering angle, and 0 and 180° represent the forward and backward scattering angles respectively. A normalized scattering diagram as a function of ($x \cdot \sin\theta$) is shown in Figure 18.

The amount of the forward-scattered light entering a detector's field of view of can be calculated by integrating eq 15 over the acceptance angle of the detector. For a circular detector that subtends half-angle $\bar{\theta}$ at a particle ($\Omega_{acc} = 2\bar{\theta}$), the equation becomes

$$\frac{2\pi x^4}{k^2}\int_0^{\bar{\theta}}\left[\frac{J_1(x\sin\theta)}{x\sin\theta}\right]^2 \sin\theta\, d\theta. \qquad (16)$$

Integrating eq 16 and then normalizing, one obtains the following

$$F = \left[1 - J_0^2(x\sin\bar{\theta}) - J_1^2(x\sin\bar{\theta})\right] \qquad (17)$$

where F is the relative amount of the diffracted light collected by a detector, and J_0 and J_1 are Bessel

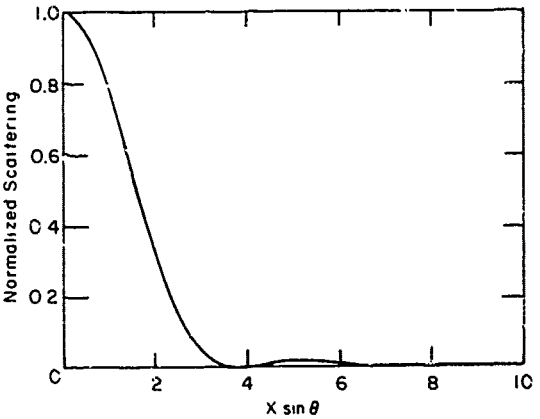

Figure 18. Normalized scattering in the near-forward direction for a spherical particle calculated using the Fraunhofer diffraction theory.

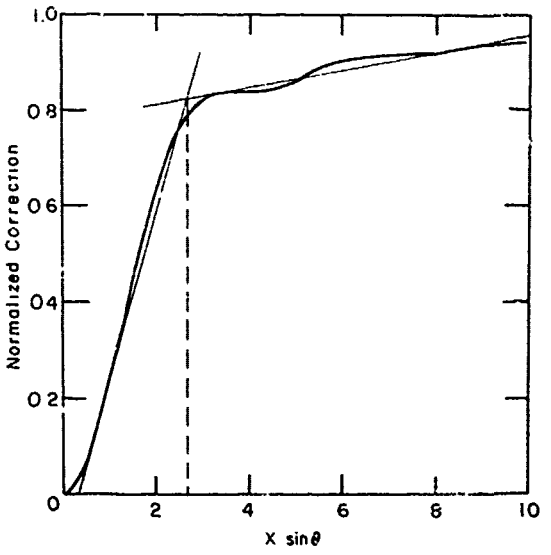

Figure 19. Relative amount of the diffracted light collected by a detector calculated as a function of the size parameter and the angle subtended by a detector. Linear approximation is also shown.

functions of order 0 and 1 respectively. The value of F as a function of $(x \cdot \sin\theta)$ is shown in Figure 19. The figure also illustrates that eq 17 can be simplified by a linear approximation where

$$F = 0.3\,(x \sin\bar{\theta}) \qquad x \sin\bar{\theta} < 2.7 \qquad (18a)$$

$$F = 0.8+0.15\,(x \sin\bar{\theta}) \qquad x \sin\bar{\theta} > 2.7 \qquad (18b)$$

Since the acceptance angle of a typical transmission system is very small, the value of F can, in most cases, be approximated by eq 18a.

The value of F expressed in eq 18 is appropriate for a single particle. The calculation for the mean value of the fraction of diffracted light $\bar{F}$ collected by a detector during transmission measurements requires lengthy integration since F depends on the size of the snow particle and on the location of the particle along the transmission path. To avoid the lengthy integration, the value for $\bar{F}$ was approximated to be equivalent to the value of F calculated for the mean particle size located at the midpoint of the transmission path.

Since one-half of the extinction cross section is attributable to the diffraction, the relationship between the "measured" and the "theoretical" extinction coefficient is given by

$$\hat{B}_{ext} = B_{ext}\,(1-0.5\,\bar{F})$$

where $\hat{B}_{ext}$ is the measured extinction coefficient. As expected, $\hat{B}_{ext}$ approaches the theoretical as the amount of the forward-scattered light that is collected by a detector becomes increasingly smaller.

Bohren and Koh (1985) investigated the forward-scattered correction required for nonspherical particles. Prolate and oblate spheroids were used to model the shape of the snow particles. A spheroid is formed by rotating an ellipse about one of its axes; therefore, the projection of a spheroid onto a plane is an ellipse. The differential scattering cross section for a spheroid in the near forward direction is given by

$$\frac{dC_{sca}}{d\Omega} = \frac{x^4}{k^2}\left[\frac{J_1(x\gamma\sin\theta)}{(x\gamma\sin\theta)}\right]^2 \qquad (20)$$

where $\gamma = \left[(\alpha/\beta)\cos^2\phi + (\beta/\alpha)\sin^2\phi\right]^{1/2}$.

If a and c are the semimajor and the semiminor axes of the spheroid, the semimajor α and the semiminor β axis lengths of the corresponding projected ellipses for prolates are

$$\alpha = (a^2\sin^2\theta + c^2\cos^2\theta)^{1/2}$$

$$\beta = c$$

and for oblates,

$$\alpha = a$$

$$\beta = (a^2\sin^2\theta + c^2\cos^2\theta)^{1/2}.$$

ϕ is the angle that the major axis makes with the normal to the plane onto which the spheroid is projected. The size parameter x is $k\sqrt{\alpha/\beta}$.

If the spheroid is randomly oriented, the scattering must be averaged over all possible rotations of the spheroid. The average differential scattering cross section then becomes

$$\left(\frac{dC_{sca}}{d\Omega}\right) = \int_0^{2\pi}\int_0^{\pi} P(\Theta,\Phi)\,\frac{dC_{sca}}{d\Omega}\sin\Theta\,d\Phi \qquad (21)$$

where $P(\Theta, \Phi)$ is the probability distribution of the spheroid orientation. These calculations indicate that the fraction of the forward-scattered light is less for nonspherical particles than it is for the equivalent sphere approximation.

Precipitation rate and extinction

The snow precipitation rate can be approximated by

$$R_S = \int_0^{\infty} \frac{n(a)\,v(a)\,m(a)\,da}{\rho_w} \qquad (22)$$

where $v(a)$ = fall velocity
$m(a)$ = mass of snow
ρ_w = density of water.

Combining eq 12 and 22, one can express the relationship between the extinction coefficient and the snow precipitation rate as

$$B_{ext} = k \cdot R_S \qquad (23)$$

where k is equal to

$$k = \rho_w \frac{\int_0^{\infty} 2\pi a^2 n(a)\,da}{\int_0^{\infty} n(a)\,v(a)\,m(a)\,da} \qquad (24)$$

Since the size, the fall velocity and the mass of snow particles vary from one snowfall to another, a range of values for k is expected, with lower k values being associated with heavy, fast-falling particles.

Numerous empirical studies to determine values for k have been conducted by simultaneously

measuring the extinction coefficient $\hat{B}_{ext}$ and R_s. Mason (1978) and Seagraves (1986) reviewed these empirical studies and found the results to vary widely. A summary of previously observed $\hat{B}_{ext}$ to R_s relationships is presented in Table 3. The discrepancies in these results are probably the result of different snowfall conditions, the different geometries of the transmission systems and discrepancies in the snow precipitation rate measurements.

Table 3. Relationships between measured extinction coefficient and snow precipitation rate.

$\hat{B}_{ext}=3.2\cdot R_S^{0.91}$	Poljakova and Tretjakov (1960)
$\hat{B}_{ext}=4.1\ R_S$	Lillesaeter (1965)
$\hat{B}_{ext}=2.4\cdot R_S$	Warner and Gunn (1969)
$\hat{B}_{ext}=3.1\cdot R_S$	O'Brien (1970)
$\hat{B}_{ext}=1.9\ R_S$	Nishitsuji and Matsumoto (1971)
$\hat{B}_{ext}=2.5\cdot R_S^{0.77}$	Muench and Brown (1977)

The precipitation rates for most of the above-mentioned studies were measured using mechanical snow gauges. The poor time resolution of these gauges required the data to be averaged over long periods. During the SNOW tests, the value for k was reinvestigated using electronic-balance snow gauges. Linear regression results yielded several $\hat{B}_{ext}$ to R_s relationships, which generally ranged from

$$\hat{B}_{ext} = 1.5\cdot R_S \tag{25a}$$

to

$$\hat{B}_{ext} = 7.0\cdot R_S \tag{25b}$$

These results are consistent with the previous empirical findings (Table 3). The slightly wider range of k values observed during the SNOW tests may have been caused by the shorter averaging time (1 minute) used to determine the precipitation rate. The importance of snow particle type on the $\hat{B}_{ext}$ to R_s relationship is evident by the range of values reported for k. Since the $\hat{B}_{ext}$ to R_s relationship varies widely, the precipitation rate alone is not a suitable parameter for use in the evaluation of electro-optical system performance.

Mass concentration and extinction

The snow mass concentration is the snow mass per unit volume of air. It can be approximated by

$$M_S = \int_0^\infty n(a)\, m(a)\, da\,. \tag{26}$$

The relationship between the extinction coefficient and the snow mass concentration is

$$B_{ext} = \frac{\int_0^\infty 2\pi a^2\, n(a)\, da}{\int_0^\infty n(a)\, m(a)\, da} M_S. \tag{27}$$

This expression is similar to eq 24; however, the uncertainty due to variations in $v(a)$ is eliminated. Therefore, the extinction coefficient can be more accurately estimated from the measurement of mass concentration than it can be from the snow precipitation rate measurement. This is illustrated in Figure 20 which shows the relationships between the extinction coefficient and the two snowfall parameters. The plot of the $\hat{B}_{ext}$ to M_s relationship clearly shows less scatter than the $\hat{B}_{ext}$ to R_s plot.

Empirical $\hat{B}_{ext}$ to M_s relationships have been well documented during the SNOW tests. Lacombe and O'Brien (1982) used a linear regression and found good correlation between the visible and infrared extinction coefficients and the snow mass concentration. Their results are shown in Table 4. Lacombe et al. (1983) segregated visible extinction and snow mass concentration data according to the snow type and observed improved correlation between $\hat{B}_{ext}$ and M_s. For all types of snow, a power fit curve to the data yielded the following relationship

$$\hat{B}_{ext} = 9.7\cdot M_S^{0.88}. \tag{28}$$

Hutt et al. (1986) conducted an independent study of the $\hat{B}_{ext}$ to M_s relationship. A linear regression analysis of their data yielded the following relationship:

$$\hat{B}_{ext} = k\cdot M_S \tag{29}$$

where k ranged from 12.5 to 16.7.

Snow mass extinction coefficient

A parameter that is commonly used to characterize an atmospheric obscurant is the mass extinction coefficient α_m, which is a measure of how ef-

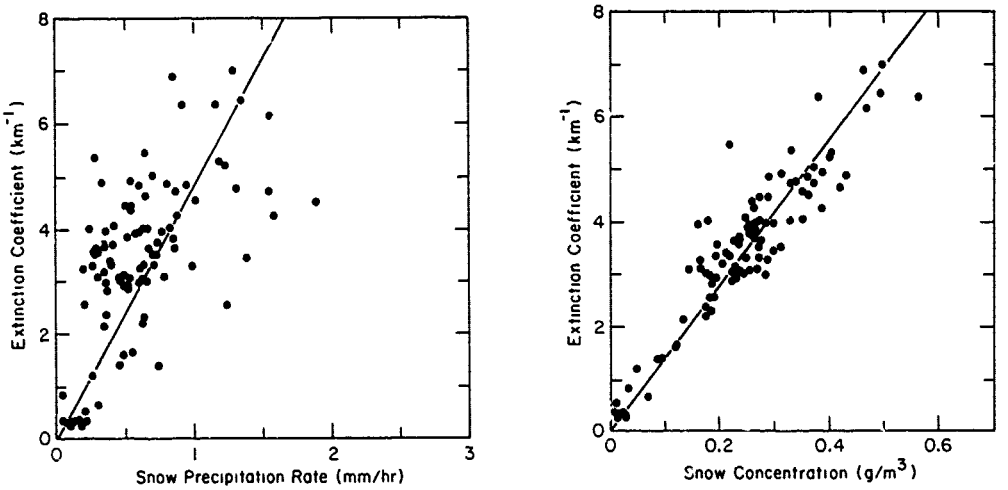

Figure 20. Comparision of the B_{ext} to M_s and B_{ext} to R_s relationships observed during a snowfall.

Table 4. Relationship between measured extinction coefficient and snow mass concentration (after Lacombe and O'Brien 1982).

Wavelength (μm)	$\hat{B}_{ext}$ = k · M_S (km^{-1})
0.55	$\hat{B}_{ext}$ = 13.41 · M_S
1.06	$\hat{B}_{ext}$ = 14.16 · M_S
3.0	$\hat{B}_{ext}$ = 19.21 · M_S
10.37	$\hat{B}_{ext}$ = 19.05 · M_S

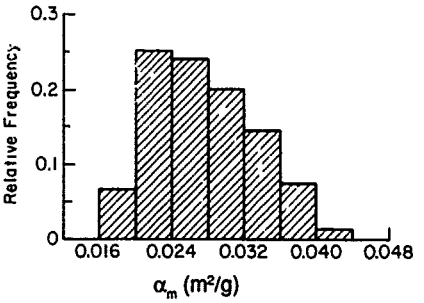

Figure 21. Distribution of the snow mass extinction coefficient for visible wavelength obtained from simultaneous measurements of snow mass concentration and visible transmittance.

fectively a fixed mass of a particle scatters and absorbs the radiation incident upon it. The relationship between the theoretical transmittance and the mass extinction coefficient is expressed as

$$T = \exp(-\alpha_m \cdot M_S \cdot L) \tag{30}$$

Equation 30 can be rearranged to

$$\alpha_m = \frac{-\ln T}{M_S \cdot L} \tag{31}$$

to show that α_m can be determined from simultaneous measurements of transmittance and mass concentration. To account for the forward-scattered light that enters the detector field of view during transmission measurements, eq 31 has to be modified in accordance with eq 14 and 19 to

$$\alpha_m = \frac{-\ln \hat{T}}{M_S \cdot L \cdot (1-1).5\bar{F})} \tag{32}$$

where $\hat{T}$ is the measured transmittance. Koh (1986) used eq 32 to determine the frequency distribution of α_m that occurred during the SNOW tests. The distribution shown in Figure 21 indicates that 0.03 m^2/g is an appropriate value for α_m.

Multiple scattering effect

As the optical depth ($B_{ext} \cdot L$) of a snow-filled atmosphere increases, the effect of multiple scattering eventually becomes evident (nonexponential attenuation of the transmitted energy is observed). A two-stream approximation to radiative transfer can be used to derive a simple analytical expression that describes the effects of multiple scattering on the transmitted radiation as a function of the optical depth, the single scattering albedo, and moments of the phase function. Bohren (1987) derives a simple analytical expression for the transmitted radiation by assuming that the light scattered by the particles travels in two directions only, exactly forward and exactly backward. The transmitted radiation in the two-stream approximation is expressed as

$$T = \frac{1}{1 + \frac{(1-g)}{2} \cdot B_{ext}} \quad (33)$$

where the asymmetry parameter g is the mean cosine of the scattering angle.

The transmitted radiation is composed of scattered T_s and unscattered T_u components, which can be expressed as

$$T_s = T - T_u. \quad (34)$$

where

$$T_u = \exp(-B_{ext} \cdot L) \quad (35)$$

The measured transmittance $\widehat{T}$ is the sum of the scattered and unscattered radiation that enters the field of view of the detector. The measured transmittance in a multiple scattering medium can be expressed as

$$\widehat{T} = T_u + f \cdot T_s \quad (36)$$

where f is equal to the fraction of the scattered radiation in the forward direction that is measured by a detector. The value of f is dependent on the beam geometry, the optical depth and the snow asymmetry parameter. Figure 22 is a comparison of visible transmission data obtained during the SNOW tests with those calculated using eq 36. A more detailed derivation of eq 36 is given by Koh (1989).

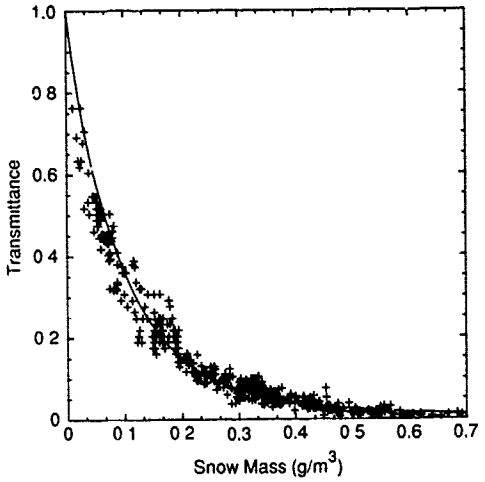

Figure 22. Comparison of the visible transmission data with those calculated using the two-stream approximation to radiative transfer.

Visibility and extinction

Snow alters the contrast of the atmosphere so that the visual range V_r decreases as the snow load in the atmosphere increases. Visual range is defined as (Middleton 1952)

$$V_r = \frac{1}{B_{ext}} \ln(C/\varepsilon) \quad (37)$$

where C is the inherent contrast of the target against the background and ε is the observer's contrast threshold. A widely used formula for characterizing the effect of the atmosphere on the performance of electro-optical devices is the Koschmieder's relationship for the meteorological range V_m. This is obtained by solving eq 37 for a black target against a horizon sky (C = 1) and assuming that $\varepsilon = 0.02$. Equation 37 then becomes

$$V_r = V_m = \frac{3.912}{B_{ext}} \quad (38)$$

where V_m is defined as the meteorological range. The meteorological range is often assumed to be the visibility (how far a person can see), so that a simple inverse relationship between extinction coefficient and visibility is assumed. This is of practical interest since the extinction coefficient may be estimated from how far an observer can see during a snowstorm.

During the SNOW tests, experiments were conducted with trained observers to measure the visibility of predetermined targets during snowfall (Lacombe and Petzko 1987). These visibility measurements were converted to extinction coefficients using the Koschmieder's relationship, and then compared with the extinction coefficients measured with a transmissometer. The results shown in Figure 23 suggest that large differences can occur.

Although the simple inverse relationship assumed between the visiblity and the extinction coefficient makes the Koschmieder's relationship an attractive tool, its practical application may be limited. The value of 0.02 for the contrast threshold is controversial and large discrepancies appear in the literature. The contrast threshold is dependent on the angle subtended by the target, the sharpness of the boundary between the target and the background, and the level of illumination. Even if these factors are held constant, there are differences among observers. In addition, the ideal black target against the horizon may not be present when the visibility measurements are made. Finally, the use of the Koschmieder's relationship is limited to daytime. At night, a light source of known intensity is required to make visibility measurements.

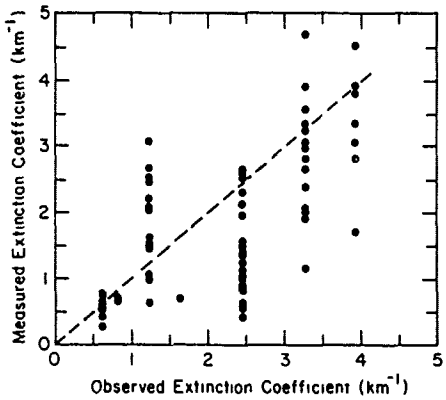

Figure 23. Comparison of the extinction coefficients estimated from visibility measurements with those measured with a transmissometer (after Lacombe and Petko 1987).

Direct measurement of extinction

Transmittance measurement is the preferred technique for determining the extinction coefficient through falling snow. However, such measurement requires a path length of several hundred meters to provide accurate results over a broad range of snowfall conditions. This makes it impractical for military application, where a simple technique to directly measure the snow extinction coefficient in an area where an electro-optical system is to be deployed is of practical interest. Extinction coefficient measurement devices that use a short path light-scattering technique may be more suited for military applications since such instruments are portable and easy to deploy.

Measurement of extinction by light-scattering is based on the principle that the intensity of the scattered light at certain angles is linearly related to the extinction coefficient. Mathematically, this relationship is expressed as

$$\frac{B_{ext}}{\int_0^{2\pi} \cdot \int_{\theta_1}^{\theta_2} 2\beta(\theta) \sin\theta \, d\theta \, d\phi} = \text{constant.} \qquad (39)$$

Since detectors for measuring light possess finite acceptance angles, the angular scattering coefficient $\beta(\theta)$ is measured over some range θ_1 to θ_2. Theoretical and experimental studies by Winstanely and Adams (1975) have shown that a forward-scatter meter can be used to measure extinction coefficient in fog using the relationship expressed in eq 39.

Experiments by Muench and Brown (1977) and Koh (1987) have shown that forward-scatter meters designed to operate in fog can also be used for measuring extinction coefficient in falling snow. A forward-scatter meter shown in Figure 24, which measures the light scattered between 27 and 47°, was used to measure extinction in falling snow, and its results were compared with the results obtained using transmission technque. Figure 25 indicates that a foward-scatter meter, once calibrated for snow, can be used to predict visible and infrared transmission through falling snow.

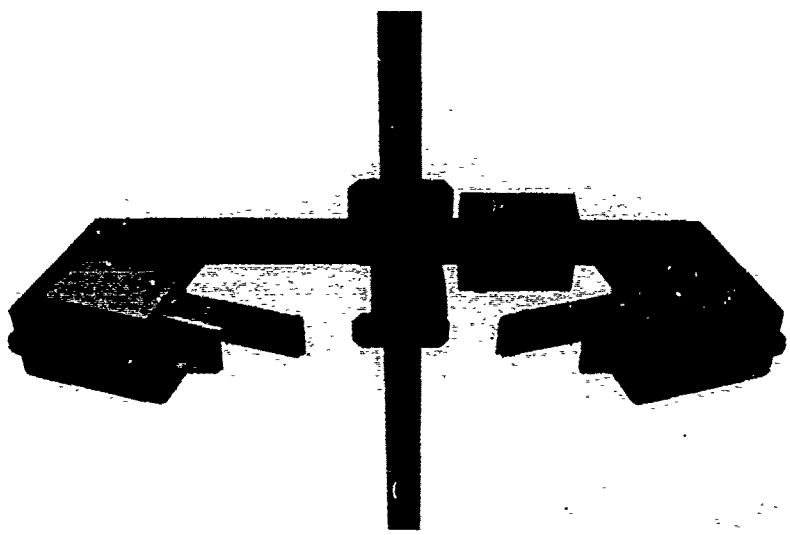

Figure 24. HSS forward-scatter meter used for measuring extinction in falling snow.

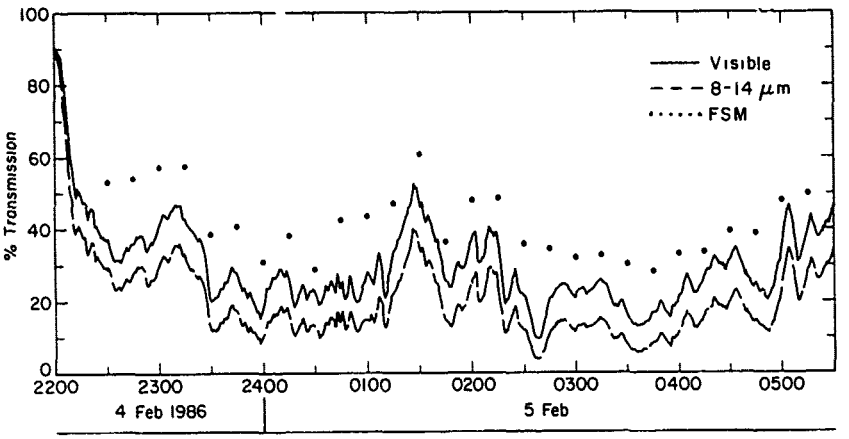

Figure 25. Comparison of the measured transmittance in the visible and infrared wavelengths with those predicted using a forward-scatter meter designed for operation in fog. A different calibration is required for snow..

CONCLUSIONS

The effect of falling snow on the performance of an electro-optical system depends on the particular system and its intended function. Snow in the atmosphere scatters and absorbs optical radiation and therefore degrades the performance of many sensors operating in a winter environment. The SNOW tests were conducted to investigate the effect of snowfall on the optical properties of the propagation path. Numerous transmittance measurements in the visible and infrared regions were made in conjunction with detailed measurements to characterize the falling snow. As a result, new empirical and theoretical models to predict the attenuation of optical radiation in falling snow and improved techniques to characterize the properties of falling snow have been developed.

More studies are required to develop a satisfactory analytical expression to describe the snow size distribution. Our inability to model the complex mechanism of snowfall formation and to accurately measure the size of snow particles has limited snow size distribution studies. Information on the phase function of snow particles is also limited. Experiments are required to measure the angular light-scattering properties of snow to more effectively address the effects of single and multiple scattering on the energy measured by any optical system.

Although much effort has been made to study the physical and optical properties of falling snow, it is necessary in the future to measure the effects of the snow-filled path in terms of the parameters that are useful in the analysis of electro-optical systems. The extinction coefficient is a general measurement of attenuation that can be applied uniformly to all electro-optical systems. However, system performance predictions may require parameters beside the extinction coefficient. Future study of the optical properties of the snow-filled atmosphere that address such parameters as the modulation transfer function, the point spread function, and time dispersion of the snow-filled atmosphere will be useful.

LITERATURE CITED

Berger, R.H. (1983) Characterization of snow for evaluation of its effect on electromagnetic wave propagation. In *Optical Engineering for Cold Environments* (G.W. Aitken, Editor). *Proceedings of the Society of Photo-Optical Instrumentation Engineers,* **414**: 35–42.

Berthel, R.O., V.G. Plank and B.A. Main (1983) SNOW-ONE-A and B characterization measurements and data analysis. Air Force Geophysics Laboratory, AFGL-TR-83-0256.

Bisyarin, V.P., I.P. Bisyarina, V.K. Rubash and A.V. Sokolov (1971) Attenuation of 10.6-μm laser radiation in atmospheric precipitation. Translated in *Radio Engineering Electronic Physics,* **16**: 1594–1597.

Bisyarin, V.P., I.P. Bisyarina, and A.V. Sokolov (1973) Temporal distribution of coefficients of attenuation of laser radiation at 0.63 μm and 10.6 μm during propagation in the troposphere. Translated in *Radio Engineering Electronic Physics,* **16**: 1632–1636.

Bohren, C.F. (1987) Multiple scattering of light and some of its observable consequences. *Ameri-*

can Journal of Physics, **55**(6): 524–533.

Bohren, C.F. and G. Koh (1985) Forward-scattering corrected extinction by nonspherical particles. *Applied Optics*, **24**: 1023–1029.

Duncan, L.D. (1981) EOSAEL 80, Volume I, Technical Documentation. U.S. Army Atmospheric Sciences Laboratory, ASL-TR-0072.

Feng, D. and L.O. Grant (1982) Correlation of snow crystal habit, number flux and snowfall intensity from ground observations. In *Extended Summaries of Conference on Cloud Physics, American Meteorological Society*, p. 485–86.

Gunn, K.L.S. and J.S. Marshall (1958) The distribution with the size of aggregate snowflakes. *Journal of Meteorology*, **15**: 452–461.

Holroyd, E.W.,III (1986) Surface sampling of a snowstorm by a 2D-C probe with and without aspiration. *Journal of Atmospheric and Oceanic Technology*, **3**: 755–758.

Houghton, H.G. (1986) *Physical Meteorology*. Cambridge: The MIT Press.

Humphries, J.H. (1985) Application of an airborne optical array probe for ground-based microphysical observations. *Journal of Atmospheric and Oceanic Technology*, **2**: 252–259.

Hutt, D.L., L.R. Bissonette and J. Oman (1986)The measurement of airborne snow mass concentration. Defense Research Establishment, Valcartier, Canada, R-445/86.

Jiusto, J.E. and G.E. Bosworth (1971) Fall velocity of snowflakes. *Journal of Applied Meteorology*, **10**: 1352–1354.

Koh, G. (1986) Snow mass extinction coefficient. In *Proceedings of Snow Symposium V*. USA Cold Regions Research and Engineering Laboratory, Special Report 86-15.

Koh, G. (1987) Extinction coefficient measurement in falling snow with forward scatter meter. USA Cold Regions Research and Engineering Laboratory, Special Report 87-4.

Koh, G. (1989) Radiative transfer in falling snow: A two-stream approximation. USA Cold Regions Research and Engineering Laboratory, CRREL Report 89-6.

Koh, G., and J. Lacombe (1986) Optical snow precipitation gauge. In *Proceedings of the Eastern Snow Conference*, 43rd Annual Meeting, Hanover, NH, p. 26–31.

Koh, G., J. Lacombe and D.L. Hutt (1988) Snow mass concentration and precipitation rate. *Cold Regions Science and Technology*, **15**: 89–92.

Lacombe, J. (1983) Technique for measuring the mass concentration of falling snow. In *Optical Engineering for Cold Environments* (G.W. Aitken, Ed.). *Proceedings of the Society of Photo-Optical Instrumentation Engineers*, **414**: 17–28.

Lacombe, J. and H.W. O'Brien (1982) Visible and infrared attenuation in falling snow. In *Proceedings of Smoke/Obscurant Symposium VI*, OPM Smoke/Obscurant Report DRCPM-SMK-T-001-82.

Lacombe, J., G.Koh, and J.A. Curcio (1983) Visible propagation in falling snow as a function of mass concentration and crystal type. In *Proceedings of SNOW Symposium II*. USA Cold Regions Research and Engineering Laboratory, Special Report 83-4.

Lacombe, J. and D.R. Petzko (1987) Winter validation of EO sensor target detection algorithms. In *Proceedings of the Eighth Annual EOSAEL/TWI Conference*, Vol. III. USA Laboratory Command, Atmospheric Sciences Laboratory.

Lillesaeter, O. (1965) Parallel-beam attenuation of light, particularly by snow. *Journal of Applied Meteorology*, **4**: 607–613.

Locatelli, J.D. and P.V. Hobbs (1974) Fall speeds and masses of solid precipitating particles. *Journal of Geophysical Research*, **79**: 2185–2197.

Magono, C. (1951) On the fall velocity of snowflakes. *Journal of Meteorology*, **8**: 199–200

Magono, C. (1953) On the growth of snow flake and graupel. *Science Reports of the Yokohama National University*, Section 1, No. 2, 18–24.

Magono, C. (1954) On the falling velocity of solid precipitation elements. *Science Reports of the Yokohama National University*, Section 1, No. 3, 33–35.

Magono, C. and C.W. Lee (1966) Meteorological classification of natural snow crystals. *Journal of Faculty of Science, Hokkaido University*, **2**: 321–335.

Mason, J.B. (1978) Light attenuation in falling snow. USA Atmospheric Sciences Laboratory, ASL-TR-0018.

Mellor, M. (1966) Light scattering and particle aggregation in snowstorms. *Journal of Glaciology*, **6**: 237–248.

Mellor, M. (1983) Snow concentration and effective air density during snowfalls. *Journal of Glaciology*, **29**: 503–507.

Middleton, W.E.K (1952) *Vision Through the Atmosphere*. Toronto: University of Toronto Press.

Mill, J.D. and E.P. Shettle (1983) A preliminary LOWTRAN snow model. In *Proceedings of SNOW Symposium II*. USA Cold Regions Research and Engineering Laboratory, Special Report 83-4.

Miller, J.T. (1978) Experimental laser attenuation in a snow environment. Arnold Engineering Development Center, AEDC-TR-7799.

Muench, H.S. and H.A. Brown (1977) Measurement of visibility and radar reflectivity during snowstorms in the AFGL Mesonet. U.S. Air Force

Geophysics Laboratory, AFGL-TR-77-0148.
Nakaya, U. (1954) *Snow Crystals*. Cambridge, Mass.: Harvard University Press.
Nishitsuji, A. and A. Matsumoto (1971) The character of falling snow. In *Monograph Series of Research Institute of Applied Electronics*, no. 19, Hokkaido University.
Norment, H.G. (1986) Numerical studies of sampling efficiencies of the ASCME and PMS aspirator hydrometeor measurement instruments. In *Proceedings of SNOW Symposium V*. USA Cold Regions Research and Engineering Laboratory, Special Report 86-15.
O'Brien, H.W. (1970) Visibility and light attenuation in falling snow. *Journal of Applied Meteorology*, 9: 671–683.
Poljackova, E.A. and V.D. Tretjakov (1960) Visibility in falling snow. *Glavnaya Geofizicheskaya Observatoria, Leningrad Trudy*, **100**: 53–57. (Translation TT63-19744, CFSTI.)
Rosinski, J., C.T. Nagamoto and G. Langer (1983) The distribution of fall speeds and masses of ice particles in snowstorms. *Journal de Recherches Atmospheriques*, **17**: 107–120.
Schaefer, V.J. (1941) A method for making snowflake replicas. *Science*, **93**: 239–240.
Seagraves, M.A. (1983) Visible and infrared transmission and precipitation rate in falling snow. Ph.D. Thesis, Colorado State University.
Seagraves, M.A. (1986) Visible and infrared extinction in falling snow. *Applied Optics*, **25**: 1166–1169.
Seagraves, M.A. and J.F. Ebersole (1983) Visible and infrared transmission through snow. *Optical Engineering*, **22**: 90–93.
Sekhon, R.S. and R.C. Srivastava (1970) Snow size spectra and radar reflectivity. *Journal of Atmospheric Sciences*, **27**: 299–307.
Sola, M.C. and R.J. Bergman (1977) Multi-spectral propagation measurement through snow. In *Technical Digest, Topical Meeting on Optical Propagation Through Turbulence, Rain and Fog*. Optical Society of America.
Stallabrass, J.R. (1976) The airborne concentration of falling snow. National Research Council, OME/NAE Quarterly Bulletin.
Suzuki, M., S. Kokusho, E. Hide-aki and A. Akiba (1981) New method for measuring snowflake size and falling velocity. *Journal of the Japanese Society of Snow and Ice*, **43**(1): 1–8.
van de Hulst, H.C. (1957) *Light Scattering by Small Particles*. New York: Wiley and Sons.
Wang, T.I., R.S. Lawrence and M.K. Tsay (1980) Optical rain gauge using a divergent beam. *Applied Optics*, **19**: 3619–3621.
Warner, G. and K.L.S. Gunn (1969) Measurement of snowfall by optical attenuation. *Journal of Applied Meteorology*, **8**: 10–121.
Winstanely, J.V. and N.J. Adams (1975) Point visibility meter: A forward scatter instrument for the measurement of aerosol extinction coefficient. *Applied Optics*, **14**: 2151–2157.

A facsimile catalog card in Library of Congress MARC format is reproduced below.

Koh, Gary

Physical and optical properties of falling snow / by Gary Koh. Hanover, N.H.: U.S. Army Cold Regions Research and Engineering Laboratory; Springfield, Va.: available from National Technical Information Service, 1989.

iv, 28 p., illus., 28 cm. (CRREL Report 89-16.)

Bibliography: p. 21.

1. Electro-optical sensors. 2. Extinction coefficient. 3. Falling snow. 4. Winter warfare. I. United States Army. II. Corps of Engineers. III. Cold Regions Research and Engineering Laboratory. V. Series: CRREL Report 89-16.